Available online at www.sciencedirect.com
ScienceDirect
Journal of Molecular Catalysis A: Chemical 271 (2007) 98–104
JOURNAL OF MOLECULAR CATALYSIS A: CHEMICAL
www.elsevier.com/locate/molcata

New theoretical insights into epoxidation of alkenes by immobilized Mn-salen complexes in mesopores: Effects of substrate, linker and confinement

Kourosh Malek [a,*], Can Li [b], Rutger A. van Santen [a]

[a] *Schuit Institute of Catalysis, ST/SKA, Eindhoven University of Technology, P.O. Box 513, 5600 MB, Eindhoven, The Netherlands*
[b] *State Key Laboratory of Catalysis, Dalian Institute of Chemical Physics, Chinese Academy of Sciences, Dalian 116023, China*

Received 31 January 2007; received in revised form 13 February 2007; accepted 16 February 2007
Available online 28 February 2007

Abstract

The origin of enantioselectivity in the epoxidation reaction of *cis*- and *trans*-methylstyrene, catalyzed by anchored oxo-Mn^{V}-salen into MCM-41 channels, is investigated by applying density functional calculations in combination with molecular mechanics methodologies. The calculations provide new insights on the importance of electronic and steric effects of the salen ligand, substrate, immobilizing linker and MCM-41 confinement. Based on the assumption that the formation of a radical intermediate is the key step along the reaction path, the calculations are performed on a catalytic surface with triplet spin-state, comprising no Mn-salen spin-crossing. We rationalize the effect of immobilization and show how that correlates with the linker and substrate choices. We show that although a *trans*-substrate has a higher level of asymmetric induction to the immobilized Mn-salen complex than that to a homogeneous catalyst, the reaction path is more in favor of the *cis*-substrate. The MCM-41 channel reduces the energy barriers and enhances the enantioselectivity by influencing geometrical distortions of the Mn-salen complex.
© 2007 Elsevier B.V. All rights reserved.

Keywords: Enantioselectivity; Mn-salen; Immobilization; Density functional theory; Heterogeneous catalysis; Nanoporous materials; Chirality

1. Introduction

Chiral Mn-salen complexes are elegant epoxidation catalysts with excellent activity and enantioselectivity for the homogeneous asymmetric epoxidation of unfunctionalized olefins [1–3]. Recently, various methods have been employed in order to heterogenize Mn-salen complexes in nanoporous materials [4–8]. These strategies include grafting of Mn-salen complexes on mesoporous materials [4], ion-exchange of Mn-salen into Al-MCM-41 [5,6], encapsulating in zeolite frameworks [7] and immobilizig onto inorganic mesoporous materials [8]. Immobilization of enantioselective catalysts into insoluble porous carriers has advanced features of product separation and catalyst recovery [2]. Such an attractive strategy, however, may affect the catalytic performance of epoxidation reaction due to a lack of cooperative interaction between the nanoporous solid and transition metal complex. Fundamental studies of the origin of communications between the organometallic complex, immobilizing agent and the nanoporous support, help not only understand the un-known chiral recognition of the epoxidation catalytic process by Mn-salen complexes, but investigating the effect on enantioselectivity of nanoporosity in general. Despite of a large number of experimental and theoretical studies employed to investigate the origin of the enantioselectivity of homogeneous Mn-salen based catalysts [1], less efforts have focused on heterogeneous asymmetric epoxidation. More systematic theoretical and computational studies are necessary in order to understand the effect of nanoporosity and linkers on the catalytic activity of the immobilized Mn-salen complexes.

Because of their hydrothermal stability and tuneable nanoporosity, MCM-41 materials are the most applicable supports for the immobilization of Mn-salen complexes [5,6,8,9]. Recently, Mn salen complexes have been successfully immobilized into MCM-41 nanopores, using a phenoxyl or phenylsulfide group as the immobilization linker [8,9], Fig. 1. It has been recently demonstrated that when Mn-salen complex is immobilized through phenoxyl group, excess enantioselectivity (ee) for the epoxidation of *cis*-β-methylstyrene is three times more than that

* Corresponding author.
E-mail address: k.malek@tue.nl (K. Malek).

1381-1169/$ – see front matter © 2007 Elsevier B.V. All rights reserved.
doi:10.1016/j.molcata.2007.02.037

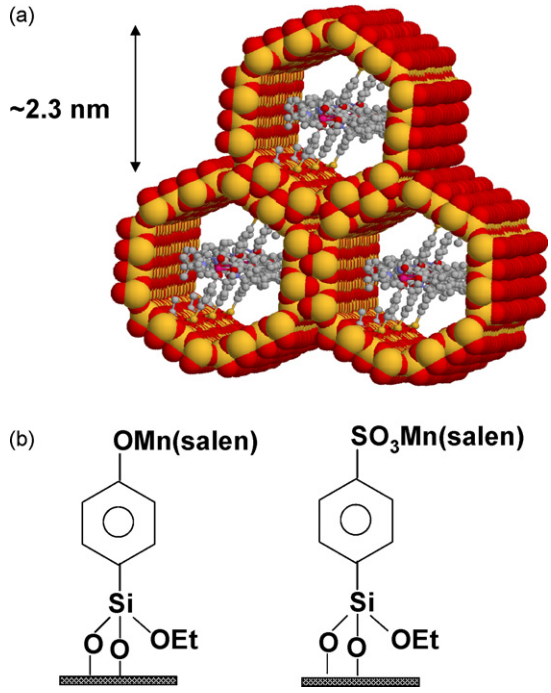

Fig. 1. (a) Visualized Mn-salen complexes anchored inside a MCM-41 channel using phenoxyl group as the immobilizing linker. (b) The model for the immobilized Mn-salen complexes using different axial linkages.

for its homogeneous counterpart. Replacement of the linker by a phenylsulfonic group improves this ratio upto 3.6 for the similar epoxidation reaction [10,11]. In both cases, *cis*-epoxide is the major product, in contrast to the homogeneous catalyst in which the *trans*-epoxide is the dominant product. Accordingly, immobilized Mn-salen catalyst shows different enanioselectivity than the homogeneous catalyst for the asymmetric epoxidation of *cis*-β-methylstyrene. It was also noted that ee values increase with the length of the immobilizing linker [11]. The nanopore and linkage length were found to be the most significant factors that influence the stereoselectivity of the immobilized Mn-salen catalysts. It was suggested that a longer linker highlights the confinement effects and subsequently enhances the enantioselectivity [10]. The mesoporous environment influences the structure of the ligand, however, it may not necessarily change the epoxidation mechanism. Apart from stereochemistry of linker and mesopore, it is of vital importance to understand the effect of *cis*- or *trans*-(Z or E) olefin as the substrate. Two main approach trajectories (side-on versus top-on) have been proposed to explain the degree and type of enantioselective communications between olefin and Mn-salen catalyst [12]. When the side-on mechanism is involved, *trans*-alkenes are generally believed to be poor substrates with homogeneous Mn-salen catalysts. It is questionable, however, if this argumentation holds for the case of the Mn-salen catalyst immobilized into a confined environment such as MCM-41.

The first principle calculations described here, expatiate on the stereo-chemical effects of the substrate (*cis*- and *trans*-β-methylstyrene), mesoporous framework and immobilizing linker into catalytic cycle and mechanism of epoxidation reaction. The enantioselectivity of immobilized Mn-salen complexes on MCM-41 channels is the result of a complex reaction–diffusion process. Different diffusion limitations influence the selective adsorption of one of the stereoisomers of substrates or products on the salen complex [2]. The mechanism of enentioselective induction for this catalytic system is not well known from microscopic point. This implies that a deep understanding of the mechanism of the epoxidation reaction, involves a careful description of the system from micro- to *meso*- and upto macro-scales. Here we focus on first-principle calculations, whereas more mesoscopic descriptions will be appeared in a future paper. Based on density functional theory (DFT) and quantum-mechanic/molecular-mechanic (QM/MM) calculations, we wish to rationalize the effect of applicable linkers and substrates in terms of their geometry and electronic properties, and evaluate the enantioselectivity of the catalyst with respect to the energy surfaces along the epoxidation reaction pathway.

2. Computational methodology

Oxo-Mn^{V}(salen)-L species, as the reaction intermediate responsible for the epoxidation, is assumed as the main reactant throughout this paper, Scheme 1. Some experimental evidence has recently been provided for this catalytically active species [13]. L is an axial ligand connected to Mn, which refers to Cl and phenoxyl for homogeneous and heterogeneous catalyst, respectively. Before we describe our method, a few remarkable concerns from previously used methodologies in the literature should be addressed. Recently, efforts in developing DFT-based computational techniques have explored ways to improve the utilization of the epoxidation reaction using Mn-salen complexes [1,14–20]. The central theme for most of those recent studies was to evaluate the accuracy of the computational methods used for epoxidation reactions catalyzed by homogeneous Mn(salen) complexes. The effect of oxo-Mn^{V}multiplicity, spin crossing dilemma and its effect on reaction intermediates have been demonstrated accordingly. Up to the present, however, no clear description of either the spin of Mn^{V}=O or the reaction intermediates has been provided [21]. Some calculations suggest that triplet state is the lowest in energy and that metallocyclic intermediate is not involved in the reaction, while presence of a radical intermediate is evident [20]. It was generally accepted that the choice of calculation method (DFT versus HF), inadequate basis sets for geometry optimization (hybrid B3LYP versus pure BP86) as well as the choice of model system for salen ligand (truncated versus full ligand, Scheme 1) are responsible for many of the contradictions reported in the

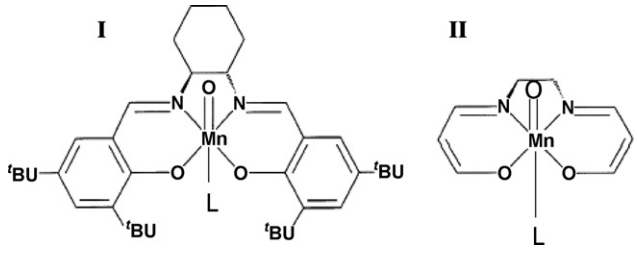

Scheme 1. The full (I) and truncated (II) models of the Mn-salen complex.

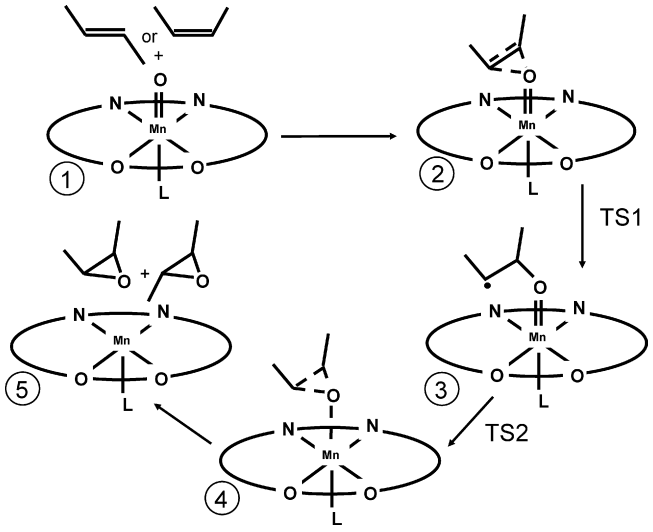

Scheme 2. General mechanism scheme for asymmetric epoxidation of olefins using Mn-salen complexes, L = axial linker.

literature [20,21]. Here, we limited ourselves to a generally accepted reaction mechanism (Scheme 2) on a triplet surface.

Pure QM calculations use a reduced model system II (Scheme 1) that mimics the full Mn(salen) complex I, along with the Cl or phenoxyl group as the axial linker L. Density functional calculations were performed with the B3LYP hybrid functional [22] in combination with 6-31G* [23] using GAUSSIAN 03 [24]. For all DFT calculations, a convergence criterion of 1.0×10^{-6} au was adopted for changes in energy and density matrix elements. Local minima on the potential energy surface were characterized by real frequencies, while transition states were characterized by an imaginary frequency, corresponding to a displacement along the reaction coordinate. All of the stationary structures on the potential energy surface and along the reaction pathway were employed to our calculations. The structures contain the isolated oxo-Mn^{V}(salen)-L intermediate and *cis*- or *trans*-β-methylstyrene (as substrates, which for the sake of convenience are referred to as CBMS and TBMS, respectively) (1), reaction intermediate complex of catalyst and substrate (2), radical intermediate of catalyst-substrate complex (3), complex of reacted catalyst and product (4), deoxygenated Mn^{V}(salen)-L catalyst, *cis*- or *trans*-epoxide (as products) (5) and the corresponding transition states (TS1 and TS2). Transition state geometries were obtained by bimolecular QTS3 method [24]. A transition state was characterized by the frequency calculations, which yielded only one imaginary frequency and independent monitoring of the imaginary frequency vibrational mode was established by using GaussView [25]. A two-layer ONIOM protocol was used to couple the QM and MM parts in the full Mn-salen-L (Scheme 1, L = pheoxyl) calculations as well as for the immobilized Mn-salen catalyst into MCM-41 channel. MCM-41 silica channel was modelled based on a straight, three-dimensional channel, Fig. 1 a. The structure was represented by the pseudo cell, Si_6O_{12}, consists of hexagon arrangements of Si–O–Si units. Oxygen atoms saturate all silicon atoms at the pore surface. Oxygen atoms with fewer than two silicon atoms attached to them (at the inlet, outlet and outer surface) were then saturated by hydrogen atoms. This model places the silicon and oxygen atoms in a simple geometrical arrangement and does not reproduce the real amorphous structure of MCM-41. In our MCM-41 model, all hydroxyl groups were located at the outer surface. The pore length is 3.4 nm and the pore diameter is 2.3 nm. Immobilization was performed by attaching the Si atom of the linker to oxygen atoms connected to two Si atoms on the wall (Si_{Linker}–O–Si_{MCM}). The UFF force field was used for the MM potentials [24]. To avoid the deformation by the attractive part of the Lennard–Jones potential, MCM-41 atoms in our QM/MM calculations were position restrained by a force of 1000 kJ mol^{-1} nm^{-2}.

3. Results and discussions

Different sets of DFT calculations are performed on all species along the reaction pathway (Scheme 2). For most of the calculations, the truncated salen ligand II is used as the model ligand, attaching to Cl or phenoxyl group. The complex Mn-salen-Cl refers to the homogeneous catalyst. The Mn-salen-phenoxyl implies the heterogeneous catalyst, where phenoxyl group is used as an immobilization linker [8,10,11]. Besides, the effect of MCM-41 mesopore attached to the phenoxyl linker, as well as the effect of *t*-butyl substituent ligands in the full salen ligand I is examined by independent QM/MM calculations based on two-layer ONIOM methodology. The QM/MM calculations are carried out on full ligand I, isolated or attached to the MCM-41 framework. The QM/MM results are presented for all the species along the reaction mechanism. By means of those calculations and in comparison with homogeneous catalyst, we intend to predict how the transition states TS1 and TS2 and intermediates 2 and 3 are stable along the epoxidation reaction pathway (Scheme 2). Particularly, we wish to describe and qualify the entioselectivity of the immobilized Mn-salen complexes for the epoxidation of CBMS and TBMS. The analysis will be performed in terms of the geometry (*cis*- versus *trans*-) of the reactants and products, effect of substituents *t-butyl* and equatorial ligands and the effect of immobilizing linker and mesoporous framework.

We have compared the optimized structure of the intermediate oxo-Mn-salen II with Cl at the *trans*-position to those where this position is occupied by phenoxyl linker. Table 1 shows the effect of the linker on the relative energies of the different spin states, calculated by the Mn triple-ξ basis using B3LYP/6-31G* functional. In the presence of both Cl and phenoxyl linkers, the triplet state is found to be the ground state [16,17]. Consequently, we assume that epoxidation reaction for both homogeneous catalyst (i.e., Cl is the axial ligand) and heterogeneous catalysts

Table 1
Relative energies of spin states for oxo-Mn-salen II complex vs. axial linkage

Method	Spin state	Mn-salen-Cl (truncated)	Mn-salen-phenoxyl (truncated)
B3LYP	Singlet	10	50
B3LYP	Triplet	0	0
B3LYP	Quintet	2	10

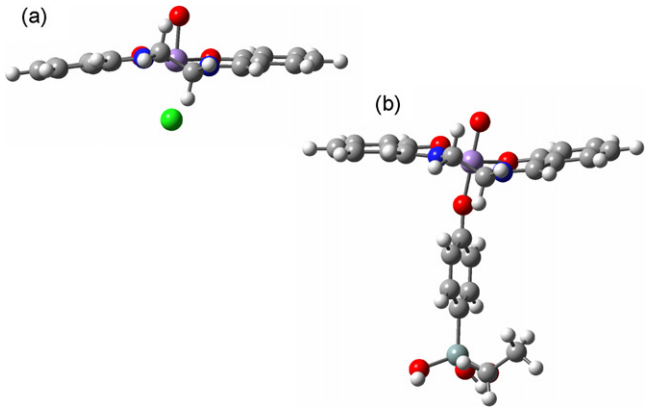

Fig. 2. DFT-calculated optimized structures for the truncated oxo-Mn-salen II with (a) Cl^- and (b) phenoxyl, located *trans*- to the oxo group.

(i.e., phenoxyl group is the axial ligand) occurs on a triplet surface. Nevertheless, the reader is referred to the literature for a detailed account of spin-crossing along the reaction pathway [1,20,21]. The reaction was suggested to proceed on at least two different spin surfaces, although recent studies showed that density functional method would affect such a spin-crossing [20,21]. A definite answer as to what DFT method is appropriate to accurately describe the mechanism of Mn-salen catalyzed epoxidation reaction, is as yet unanswered [21].

The calculated structures of the model complex II attached to each axial ligand and for the triplet ground state are illustrated in Fig. 2 and the structural parameters are summarized in Table 2. It has already been suggested that any coordination in the *trans*-position causes the Mn atom to move into the plane of the ligand [26]. In addition, the Mn= O bond becomes lengthened. As part of a side-on mechanism, the movement of the Mn atom can enhance the enantioselectivity by affecting the shielding of the oxygen by the equatorial ligands. The effect of axial donor ligand on the downward motion of the Mn atom is more remarkable than the lengthening of the Mn= O bond. The latter indicates that the axial ligand weakens the Mn= O bond and facilitates oxygen transfer to the olefin. Table 2 shows that phenoxyl group has more effect on the Mn= O bond length than Cl. An electrophilic linkage, lengthened through introduction of aliphatic chains [10], affects the geometry of the salen ligand in terms of Mn=O bond length and Mn atom motion. This may explain the higher ee observed in the recent experimental studies by a long phenylsulfonic linker [9–11]. The longer axial linker, however, may decrease the degree of electronic communication between the mesoporous support material and salen ligand, which will

Table 2
Effect of axial linkage on the geometry of oxo-Mn-salen II for the triplet spin sate using B3LYP method: distances in Å, angles in degrees

Bond/angle	Mn-salen-Cl (truncated)	Mn-salen-phenoxyl (truncated)
Mn= O(oxo)	1.82	2.11
Mn— O(phenoxyl)	2.34	1.85
Ligand plan . . . Mn	0.184	0.555
∠Mn–O(oxo)–L	56.94	124.93

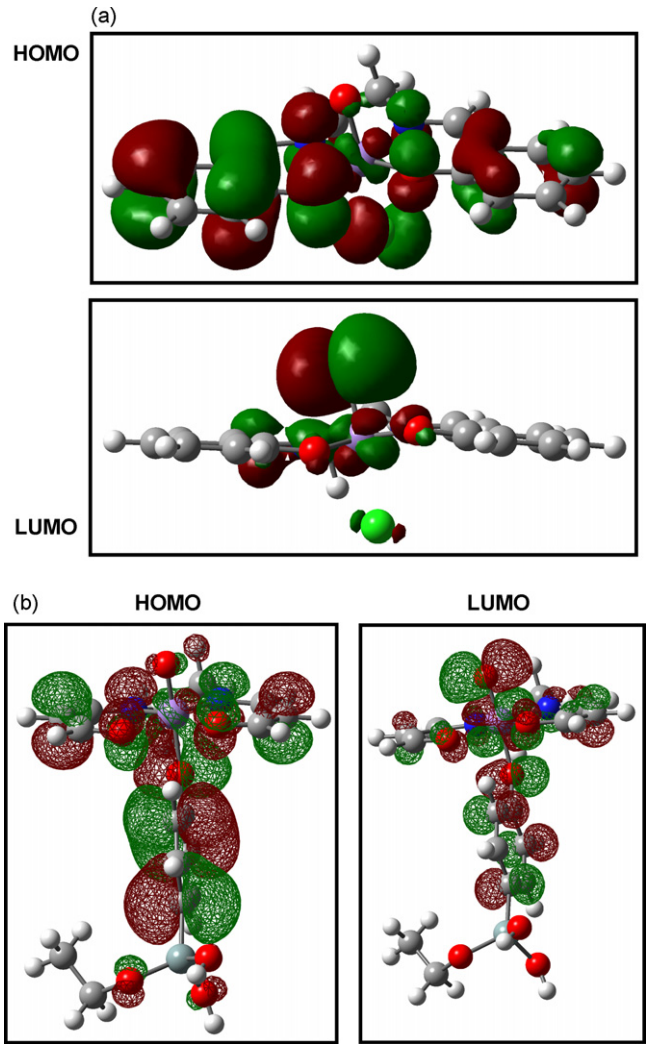

Fig. 3. DFT-calculated LUMO and HOMO states for the truncated oxo-Mn-salen II with (a) Cl^- and (b) phenoxyl, located *trans*- to the oxo group.

have a negative effect on enatioselectivity enhancement by axial linker. It is also important to notice that these local geometrical effects are accompanied by large scale conformational changes in the ligand. The latter would further increase the enantioselectivity of the catalyst by improving the chirality content of the Mn-salen ligand [27,28]. In order to provide a more orbital-based explanations and in analogy with [26], we consider the higher occupied molecular orbital (HOMO) and lower unoccupied molecular orbital (LUMO) of the Mn-salen structure II in the presence of Cl and phenoxyl axial linkages. Fig. 3 shows the HOMO and LUMO configurations for the homogeneous and heterogeneous catalyst of truncated ligand II. In the triplet state, the HOMO of the intermediate II is usually localized in d_{xy} type orbital (Mn= O is directed along z-axis). The LUMO, on the other hand, is the Mn= O π^* orbital [26]. It appears that the addition of Cl and phenoxyl axial ligands does not affect the configuration of HOMO and LUMO. When the CBMS or TBMS approaches the Mn= O by means of a side-on trajectory, a good overlap of the olefin's HOMO with complex's LUMO determines the reactivity and enantioselectivity of the complex.

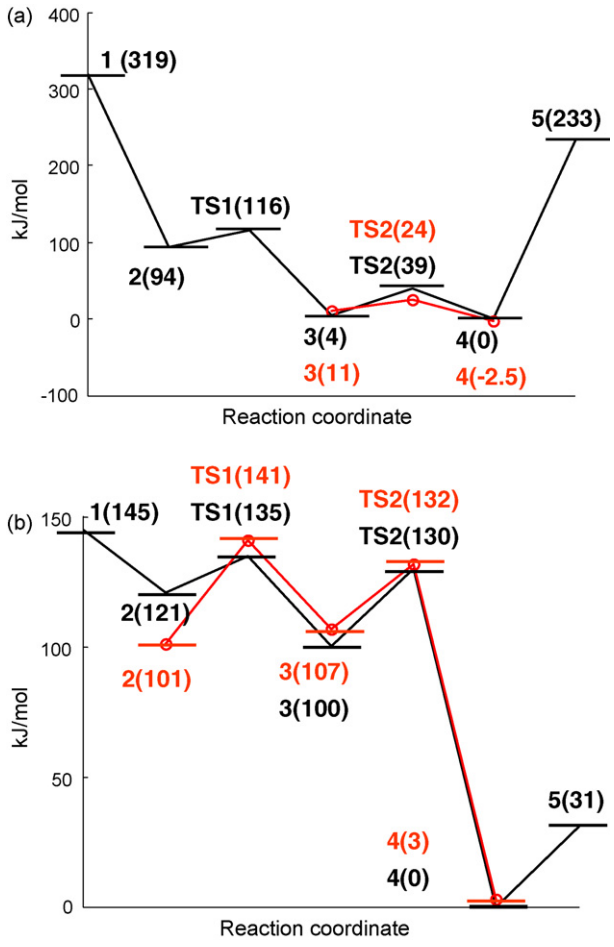

Fig. 4. Reaction profiles for the oxygen transfer reaction on the triplet surface for (a) homogeneous and (b) heterogeneous Mn-salen catalyst. The species are defined as in Scheme 2. The (black) full line refers to the energy profile for the attack of CBMS, while the (red) dotted line is the profile of TBMS attack. The relative energies are shown in parentheses. (For interpretation of the references to colour in this figure legend, the reader is referred to the web version of the article.)

The nature of axial linkage (electrodonor versus electroacceptor) will affect this type of interactions between *cis*- or *trans*-olefin and the Mn=O catalytic center.

The energetics of reaction sequence for the transformation of CBMS and TBMS into *cis/trans*-epoxide is illustrated in Fig. 4 a and b. In principle, there are four possible trajectories for olefin attack at the Mn= O center and in the framework of a side-on approach [19]. An skew angle, $\angle\phi$ = (Mn–O–C(CH_3)–C(Ph)), was introduced to measure the deviations from the idealized parallel side-on approach. The olefin attacks at $\phi = -90^\circ$ is a suitable angle as the attacks from $\phi = 0^\circ, 90^\circ$ and 180° angles are 10–20 kJ/mol higher in energy [19]. First, we consider the energy profile for the homogeneous epoxidation reaction of *cis*-β-methylstyren (CBMS) along the reaction pathway (Scheme 2). The reference state at 0 kJ/mol is the epoxide complex 4, in which both of the carbon atoms of the olefin are connected to the oxygen. System 1 is the mixture of CBMS and the catalyst in gas phase without any interaction in between. The state 2 refers to the system in which olefin enters the coordination sphere of complex from the Mn= O center, accounting for the side-on approach. The distance between olefin and oxygen in Mn=O was found to be 0.28 nm [18]. This system passes through the transition state TS1 and converts to the radical intermediate 3. The activation energy for this step is around 22 kJ/mol. The radical intermediate 3 is 90 kJ/mol more stable than system 2. The radical 3 can further collapses to yield the epoxide complex through a relatively high activation barrier (35 kJ/mol). Similar calculations was performed for the side-on attack of TBMS onto Mn=O center. Calculations show that the attack of TBMS is overall about 7 kJ/mol less in favor compared to that in CBMS. Moreover, Fig. 4 a illustrates that the epoxide complex 4 formed by TBMS lies 2.5 kJ/mol below the epoxide complex formed by CBMS. These findings are in agreement with a general assumption in homogeneous Mn-salen catalyst that TBMS is a less suitable substrate than CBMS. The more stable *t* rans-epoxide complex 4 is in qualitative agreement with the experimental observation that epoxidation of CBMS leads to a thermodynamically more stable *trans*-epoxide [29]. When the axial linkage is replaced by phenoxyl group, the potential energy surface changes considerably. Fig. 4 b shows the energy profile for the epoxidation reaction of CBMS and TBMS catalyzed by immobilized Mn-salen complex. Similar to Fig. 4 a, the epoxide complex is the reference state at 0 kJ/mol. On the triplet energy surface, the calculations suggest that epoxide formation is clearly more preferred by the immobilized catalyst compared to the homogeneous catalyst. The activation barrier for the formation of adsorbed CBMS radical is overall 8 kJ/mol less than that for the homogeneous salen catalyst. When comparing the epoxide complex 4 for homogeneous and immobilized catalyst, the activation energy for epoxide complex formation is about 5 kJ/mol lowered for the immobilized Mn-salen complex. These observations provide an explanation for the effectiveness and importance of additional ligand as the immobilizing linker. When Mn-salen complex is immobilized by a neutral donor ligand such as phenoxyl group, the energy barrier of the final step of product formation is significantly reduced.

DFT calculations for the attack of TBMS provide a different reaction profile than that for the homogeneous catalyst. In contrast to the homogeneous epoxidation reaction, a *trans*-olefin can be a suitable substrate for epoxidation by immobilized Mn-salen catalysts. Fig. 4 b shows that the epoxide complex 4 formed of CBMS is slightly (3 kJ/mol) more stable than its *trans*-epoxide counterpart, despite of the fact that there is a lower barrier (5 kJ/mol) towards epoxide formation starting from TBMS radical adsorbed on Mn=O center. The energy profile strongly depends on electron donor/acceptor properties of the axial linker. A different linker such as phenylsulfonic group may convert the reaction pathway towards *trans*-epoxide formation. The energy barrier is still in favor for *cis*-substrate. These features can be better explained by the geometry of the transition states. Fig. 5 a and b show the geometry of the transition states TS1 and TS2 corresponding to the attack of TBMS at the Mn= O center. There are puckered and step-like distortions compared to the flat geometry of the isolated salen ligand. These conformational changes, due to the interaction of olefin molecules and axial linkage are believed to be the source of enantioselectivity for this relatively flat complex [27,28]. Fig. 5

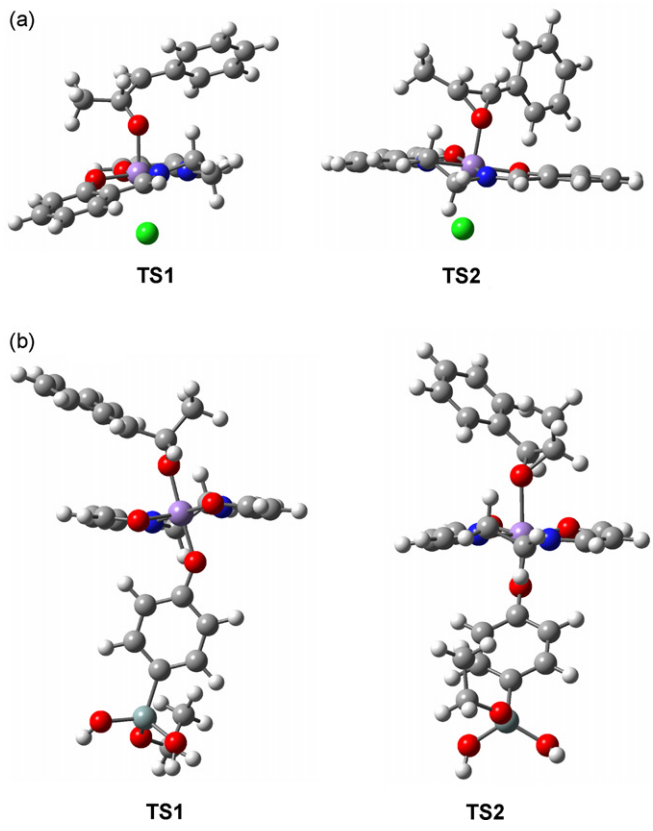

Fig. 5. Optimized geometry of TS1 and TS2 for (a) homogeneous and (b) heterogeneous Mn-salen catalyst.

shows that compared to the homogeneous case, TBMS induces more deformation on the salen ligand in the form of step-like geometry. The step-like is less pronounced in case of TBMS radical adsorbed on homogeneous salen ligand. Our calculations show that a different spin state (singlet and quintet) induces more cup-like geometry to the radical intermediate, leading to less enantioselectivity of the salen ligand. Recent experimental evidence showed that for an immobilized Mn-salen catalyst, *cis*-epoxide is the major product, compared to the homogeneous catalyst in which the *trans*-epoxide is the main product. The present calculations support this observation. However, more detailed DFT studies are essential in order to trace all of the possible intermediates. Accordingly, the capability of *t* rans-olefin as potential substrate in epoxidation reaction can not be simply inferred from the homogenous catalyst. More experimental and theoretical efforts should be focused on different enantiomeric forms of the intermediates and products along different reaction pathways, starting from *trans*- or *cis*-substrates.

Fig. 6 shows the set-up used for ONIOM-based QM/MM calculations. The high-level model system includes Mn, N, O, carbon atoms at the bridge and the full substrate and linker atoms. The low level calculation includes the rest of salen ligand and the atoms of MCM-41 channel. The energy profile for epoxidation of CBMS in this catalytic system is shown in Fig. 6. Overall, the reaction coordinates follows the same pathway as explained earlier for the axially modified salen ligand. The energy barriers are lower, most likely because of the confinement effects

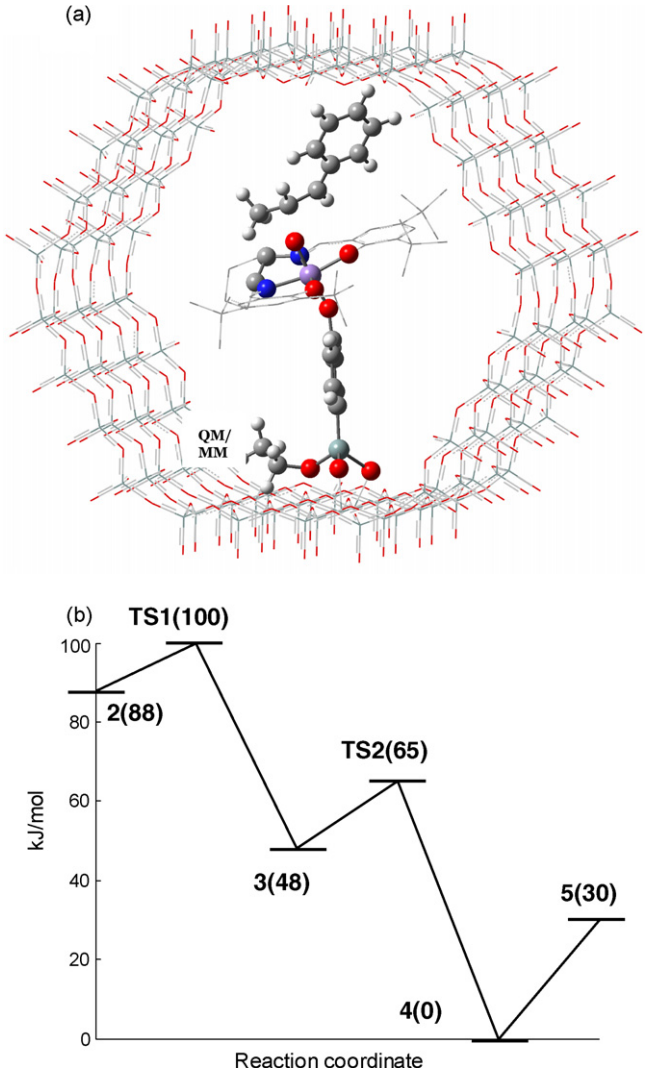

Fig. 6. (a) Representation of QM/MM system. (b) Reaction profiles for the oxygen transfer reaction on the triplet surface for Mn-salen immobilized into MCM-41 channel using a phenoxyl linker. The species are defined as in Scheme 2.

inside MCM-41 channel. The more restricted space inside the mesopore in combination with the effect of immobilizing linker hinders the free-movement of the attached olefin. The salen ligand has to be better adapted into a step-like geometry in order to minimize all these geometrical hindrances. The minima in the energy profile correspond to a constricted geometry and are due to a favorable entropy in the MCM-41 channel. Besides, a full-salen ligand with substituents at 5, 5′- and 3, 3′-positions exhibits stronger steric influences compared to that for the model complex II.

Our geometry optimizations based on DFT and QM/MM calculations, along with those of others [17,18,20] show that the intermediate 4 (Scheme 2) is the most stable species within the reaction pathway, regardless the type of axial ligand, substrate and the presence of MCM-41 confinement. We suggest that in the intermediate state 4, the olefin strongly interacts with the oxo-Mn center, with a specific high asymmetric induction to the Mn-salen complex. Besides, in the radical intermediate

3, the *cis*-configuration is more convenient because of the less steric hindrances. Once the formation of this radical intermediate is the limiting step, the implication of *cis*- or *trans*-substrate on enantioselectivity is less important. MCM-41 confinement and/or selective adsorption of one of the (stereo)isomers of the products or reactants cause a mass transfer limitation, which is another limiting factor. Our independent, preliminary free energy calculations based on grand canonical molecular dynamics simulations (GCMD) and in the presence of many anchored ligands into the MCM-41 channels, confirmed the importance of the entropy production inside the channel. However, a mesoscopic free energy calculation for the selective diffusion-adsorption processes inside a modified MCM-41 channel can address this issue further.

4. Conclusion

In order to understand the origin of enatioselectivity of an immobilized Mn-salen catalyst onto an MCM-41 channel and based on a widely accepted reaction mechanism for the epoxidation of *cis*- and *trans*-methylstyrene, we performed extensive density functional theory (DFT) and quantum-mechanics/molecular-mechanics (QM/MM) calculations. Our calculations provide new insights on the importance of the immobilized linker and the MCM-41 channel for stereoselective epoxidation of *cis*- and *trans*-methylstyrene. We analyze the consequence of immobilization in detail and show how that correlates with the electronic interactions with linker and substrates. Our DFT calculations indicate that despite of high level of asymmetric induction of *trans*-substrates to the immobilized Mn-salen complexes, the reaction path is most likely in favor for the *cis*-substrates. We have compared the optimized structure of the intermediate oxo-Mn-salen with the chloride at the *trans*-position to those where this position was occupied by a phenoxyl linker. It was suggested that any coordination in the *trans*-position causes the Mn atom to move into the plane of the ligand. In addition, the Mn= O bond becomes lengthened. According to the side-on mechanism (Scheme 1), the movement of the Mn atom can improve the enantioselectivity in view of the shielding of the oxygen by the equatorial ligands. The main finding is that immobilization by an electron-donor linker decreases the overall reaction barriers. The effect of the MCM-41 channel is important and is rather steric than electronic. The effect of channel confinement, however, strongly depends on the channel size. The results are consistent with the recent experimental studies of epoxidation reactions using heterogenized Mn-salen complexes in nanoporous materials [10,11].

Acknowledgements

We gratefully acknowledge funding by the KNAW-CAS (Royal Dutch Academy of Sciences-Chinese Academy of Sciences) international collaboration program. K.M. would like to thank Dutch Computational Facility (NCF) for providing computational time under project SG-233.

References

[1] E.M. McGarrigle, D.G. Gilheany, Chem. Rev. 105 (2005) 1563.
[2] C. Li, Catal. Rev. 46 (2004) 419.
[3] A. Corma, Catal. Rev.: Sci. Eng. 46 (2004) 369.
[4] C. Baleizao, B. Gigante, H. Garci, A. Corma, J. Catal. 221 (2004) 77.
[5] P. Piaggio, P. McMorn, C. Langham, D. Bethell, P.C. Bulman-Page, F.E. Hancock, G.J. Hutchings, New. J. Chem. (1998) 1167.
[6] P. Piaggio, P. McMorn, D. Murphy, D. Bethell, P.C. Bulman-Page, F.E. Hancock, C. Sly, O.J. Kerton, G.J. Hutchings, J. Chem. Soc. Perkin Trans. 2 (2000) 2008.
[7] C. Schuster, E. Mollmann, A. Tompos, W.F. Holderich, Catal. Lett. 74 (2001) 69.
[8] S. Xiang, Y. Zhang, Q. Xin, C. Li, Chem. Commun. (2002) 2696.
[9] H. Zhang, S. Xiang, C. Li, Chem. Commun. (2005) 1209.
[10] H. Zhang, C. Li, Tetrahedron 62 (2006) 6640.
[11] H. Zhang, Y. Zhang, C. Li, J. Catal. 238 (2006) 369.
[12] S. Chang, J.M. Galvin, E.N. Jacobsen, JACS 116 (1994) 6937.
[13] D. Feichinger, D.A. Plattner, Angew. Chem. 109 (1997) 1796.
[14] H. Jacobsen, L. Cavallo, Organometallics 25 (2006) 177.
[15] I.V. Khavrutskii, D.G. Musaev, K. Morokuma, Inorg. Chem. 42 (2003) 2606.
[16] C. Linde, B. Akermark, P.-O. Norrby, M. Svensson, J. Am. Chem. Soc. 121 (1999) 5083.
[17] L. Cavallo, H. Jacobsen, Inorg. Chem. 43 (2004) 2175.
[18] L. Cavallo, H. Jacobsen, Angew. Chem. Int. Ed. 39 (2000) 589.
[19] H. Jacobsen, L. Cavallo, Chem. Eur. J. 7 (2001) 800.
[20] L. Cavallo, H. Jacobsen, J. Phys. Chem. 107 (2003) 5466.
[21] J.S. Sears, C.D. Sherill, J. Chem. Phys. 124 (2006) 144314.
[22] C. Lee, W. Yang, R.G. Parr, Phys. Rev. B 37 (1988) 785.
[23] A. Schafer, C. Huber, R. Ahlrichs, J. Chem. Phys. 100 (1994) 5829.
[24] J.R. Cheeseman, J.A. Montgomery, Jr., T. Vreven, K.N. Kudin, J.C. Burant, J.M. Millam, S.S. Iyengar, J. Tomasi, V. Barone, B. Mennucci, M. Cossi, G. Scalmani, N. Rega, G.A. Petersson, H. Nakatsuji, M. Hada, M. Ehara, K. Toyota, R. Fukuda, J. Hasegawa, M. Ishida, T. Nakajima, Y. Honda, O. Kitao, H. Nakai, M. Klene, X. Li, J.E. Knox, H.P. Hratchian, J.B. Cross, V. Bakken, C. Adamo, J. Jaramillo, R. Gomperts, R.E. Strat-Mann, O. Yazyev, A.J. Austin, R. Cammi, C. Pomelli, J.W. Ochterski, P.Y. Ayala, K. Morokuma, G.A. Voth, P. Salvador, J.J. Dannenberg, V.G. Zakrzewski, S. Dapprich, A.D. Daniels, M.C. Strain, O. Farkas, D.K. Malick, A.D. Rabuck, K. Raghavachari, J.B. Foresman, J.V. Ortiz, Q. Cui, A.G. Baboul, S. Cliord, J. Cioslowski, B.B. Stefanov, G. Liu, A. Liashenko, P. Piskorz, I. Komaromi, R.L. Martin, D.J. Fox, T. Keith, M.A. Al-Laham, C.Y. Peng, A. Nanayakkara, M. Challacombe, P.M.W. Gill, B. Johnson, W. Chen, M.W. Wong, C. Gonzalez, J.A. Pople, Gaussian 03, Revision B01, Gaussian, Inc., Wallingford, CT, 2004, p. 17; W.F. van Gunsteren, P. Kruger, S.R. Billeter, A.E. Mark, A.A. Eising, W.R.P. Scott, P.H. Heneberger, I.G. Tironi, The GROMOS96 Manual and User Guide, Biomos and Hochschulverlag AG an der ETH Zrich, Groningen, 1996.
[25] http://www.gaussian.com.
[26] K.A. Avery, R. Mann, M. Norton, D.J. Willock, Topics Catal. 25 (2003) 89.
[27] K. Malek, A.P.J. Jansen, R.A. van Santen, J. Catal. 246 (2007) 127.
[28] K. Lipkowitz, S. Schefzick, Chirality 14 (2002) 677.
[29] N.S. Finnley, P.J. Pospisil, S. Chang, M. Palicki, R.G. Konsler, K.B. Hansen, E.N. Jacobsen, Angew. Chem. 109 (1997) 1798.